COBEM 2023 27TH INTERNATIONAL CONGRESS OF MECHANICAL ENGENEERING

ABCM Brazilian Society of Mechanical Sciences and Engineering
27th ABCM International Congress of Mechanical Engineering
December 04-08, 2023, Florianópolis-SC, Brazil

COB-2023-0163
Sound energy control in a wide frequency domain by a hybrid acoustic material

Gildean do N. Almeida
Erasmo F. Vergara
Leandro R. Barbosa
Lucas R. Zanatta
Kleyton K. Zimmermann
Robson Z. Mikulski
Victor H. P. Bahú
Laboratory of Vibrations and Acoustic, Federal University of Santa Catarina, Florianópolis, Brazil.
gildean_fsa@hotmail.com; e.f.vergara@ufsc.br; najanra.mec@gmail.com; lucasroussenqzanatta@gmail.com; kleytonkz@hotmail.com; robsonmklsk@gmail.com; victorbahu12@gmail.com

Abstract. *The evolution of acoustic materials allowed the development of structures for the control of sound energy. However, consolidating this control over a wide spectrum of frequencies is a challenging task, especially when designing structures and devices with small dimensions. In this work, a hybrid acoustic material is proposed to control sound energy in a wide range of frequencies based on the combination of a porous material layer and a modified Helmholtz resonator. Theoretical equivalent fluid models and numerical simulations using the finite element method (FEM) are used to describe the behavior of the hybrid absorber. In addition, experimental tests are conducted on an impedance tube apparatus using the standard two-microphone method. The results obtained showed good agreement. Furthermore, the bandwidth factor (Q_α) made it possible to evaluate the expanded sound energy control range. In this sense, a Q_α = 49.3% in the frequency range between 100 Hz and 3600 Hz was achieved experimentally. It was observed that the type and thickness of the porous material layer produce a strong influence on the energy control. Finally, this work contributes to the understanding the propagation of sound waves in a hybrid acoustic material, as well as to evolution of sound energy control through these materials.*

Keywords: *Sound absorption, Helmholtz resonator, Hybrid acoustic material, Equivalent fluid.*

1. INTRODUCTION

Nowadays, the control of sound energy can be obtained by differents types of acoustic materials. However, depending on the region of frequency in which desired to control, some structures absorbers stand-out more than others. For example, porous materials of celular, fibrous, granular and ceramic types have been used successfully to control of sound energy relative to high-mid-frequencies range (de Moraes *et al.*, 2019) (Doutres *et al.*, 2010) (Cao *et al.*, 2018) (Ji *et al.*, 2020) (Dupont *et al.*, 2011). On the other hand, considering the low-mid-frequencies range the micro-perforated panels (Maa, 1987) (Li *et al.*, 2017) (Cobo and Simón, 2019) (Li *et al.*, 2023), membrane type resonator (Xu *et al.*, 2022) (Mei *et al.*, 2012), traditional Helmholtz resonators (Li *et al.*, 2016) (Liu *et al.*, 2021) (Zhao *et al.*, 2018) and Helmholtz resonators with embedded necks (Huang *et al.*, 2019) (Duan *et al.*, 2020) (Mahesh *et al.*, 2021) ensure perfect control of sound energy in this region.

To acquire effective sound energy control in wide frequency domain we highlight the hybrid absorbers. In this sense, Zhang and Xin (2023) presented an coiled-up structure with porous lining, which is based on adding porous material linig on both sides of the coiled-up channel to broadband and low-frequency sound absorption. The results showed that the porous material lining not only enhances the sound energy dissipation, but also reduces the propagation speed of sound wave in the coiled channel, resulting in good low-frequency and broadband sound absorption performance of the structure. An structure metaporous with continuous high absorption within low-frequency range ($250 - 1500$ Hz) based on multi synergistic coupling effects was proposed by Xu *et al.* (2022). The authors obtained theoretical and experimentally an average absorption coefficient of 90% within $400 - 1500$ Hz with the structure presented a thickness of only 60 mm. Proposed of a compact structure based on coupling an gradient perforated porous material and coiled-up channel was presented by Li *et al.* (2022). Where an experimental control 70% of sound energy in a wide frequency range ($240 - 3000$ Hz) was obtained Furthermore, the effects of the geometry parameters of the porous material and coiled-up channel on the absorption properties was also discussed in detail. We highlight also the design of a double porosity material (DPM) composed of two types of pores, i.e., the mesopore formed by a labyrinthine channel and the traditional porous layer (Zhao *et al.*, 2020). The behavior of a absorbing structure multi band based on slit helical shape attached

to a perforated membrane backed by an air cavity (Kim and Park, 2018). The absorber with gradually perforated porous material structured by a Helmholtz resonant cavity (Liu *et al.*, 2021) and the structure composed of a perforated panel resonator and porous material (Li *et al.*, 2021).

In this work, a hybrid acoustic material (HAM) composed of the coupling between porous material layer and a Hemholtz resonator with embedded necks to guarantee to control sound energy in a wide range of frequency $(100 - 3.000$ Hz)is presented. Although this study has been motivated by the works mentioned above, the stucture proposed here differs in two aspects from the previously mentioned structures. First, unlike the structures proposed by Zhang and Xin (2023); Xu *et al.* (2022); Li *et al.* (2022) and Zhao *et al.* (2020), our HAM has a thinner thickness mainly duu to the project of the modified Helmholtz resonator. Second, unlike of structures presented by Kim and Park (2018); Liu *et al.* (2021) and Li *et al.* (2021), our geometry allows broad control sound energy in a wide frequency range. Therefore, with this strategy, it is expected to synthesize the advantages of hybrid acoustic material proposed and contribute to the undertasnding the propagation of sound waves in this material type as well as about the coupling of diferents acoustics materials for the sound energy control in a wide frequency.

This paper is organized as follows: The general aspects of the HAM and the theoretical method are presented in Section 2. A brief presentation of numerical method using the finite element method (FEM) and experimental apparatus are describes in Section 3 and 4, respectively. Sections 5 present the results and discussions. Finally, the Section 6 describes the conclusions and final remarkes the work.

2. THEORETICAL METHOD

2.1 The structure of the HAM

The hybrid acoustic material proposed consists of combined a porous layer of thickness L_f and a Helmholtz resonator (HR) with embedded necks with thickness L_t, as illustrated in Fig. 1. The resonator panel has thickness e and two square perforations, with width and height l, respectively. The perforations have thickness t. The air cavity has internal height $W = L - b$, internal width $m_i = m_e - 2b$, with m_e and b, representing the external width and thickness of the internal walls, respectivelly. The air cavity has external height L and thickness h. Finally, $a = (m_i - l - 2b)/2$ reprsents the half-width of the channel subtracted by the width of the perforation and by two internal walls.

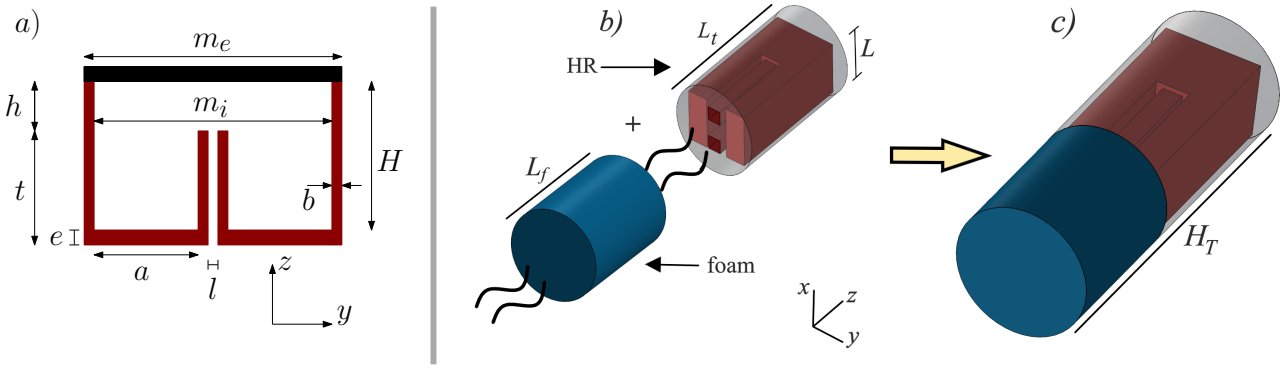

Figure 1. Schematic diagram of the HAM (foam+HR). a) Section of the Helmholtz resonantor in the plane yz. b) and c) Schematic diagram of the coupling between the foam and resonator with total thickness $H_T = L_f + L_t$, with $L_t = H + e$.

2.2 Equivalent fluid methods

The HAM absorber can be considerer as the combined of two equivalent fluid. Thus, a modified equivalent fluid (FE) approach proposed by Guo's (Guo *et al.*, 2008) is used to describes the resonator, while the Johnson-Champoux-Allard-Lafarge (JCAL) model (Johnson *et al.*, 1987); (Champoux and Allard, 1991); (Lafarge *et al.*, 1997), is applied to describes the porous layer. The total acoustic impedance of the HAM is obtained by (Kim and Park, 2018)

$$Z_h = \left[Z_f^{-1} + Z_t^{-1} \right]^{-1}, \tag{1}$$

with Z_f representing acoustic surface impedance the porous material layer and Z_t the total acoustic impedance of Helmholtz ressonator modified. Z_f is given by (Allard and Atalla, 2009)

$$Z_f = -j \frac{\sqrt{\rho_{ef} K_{ef}}}{\phi} \cot(k_{ef} L_f), \tag{2}$$

where ϕ is the filling fraction of the porous layer and $k_{ef} = \omega\sqrt{\rho_{ef}/K_{ef}}$ is the wavenumber, with ρ_{ef} representing the effective density and K_{ef} the bulk modulus. This functions are given, respectively, by

$$\rho_{ef} = \rho_0\alpha_\infty\left(1 + \frac{\eta\phi}{j\omega\rho_0\alpha_\infty q_0}\sqrt{1 + \frac{4j\alpha_\infty^2 q_0^2\rho_0\omega}{\eta\Lambda^2\phi^2}}\right), \tag{3}$$

$$k_{ef} = \frac{\gamma P_0}{\gamma - (\gamma-1)\left(1 + \frac{\phi\eta}{j\omega P_r\rho_0 q_0^{'}}\sqrt{1 + \frac{j4\omega\rho_0 P_r(q_0^{'})^2}{\eta\phi\hat{\Lambda}^2}}\right)^{-1}}, \tag{4}$$

where α_∞ is the tortuosity, Λ is the viscous characteristic length, γ =1.41 is the specific heat ratio, P_0 =101325 Pa is the atmospheric pressure, P_r =0.71 is the Prandtl number and $\hat{\Lambda}$ is the thermal characteristic length. $q_0 = \eta/\sigma_r$ and $q_0^{'} = q_0\alpha_\infty$ are the viscous and thermal permeability, respectively, with σ_r being the flow resistivity. $\eta = 1.8134\times10^{-5}$ Pa·s is the viscosity of air and $\rho_0 = 1.21$ kg·m^{-3} is the air density (for 20°C). On the other hand, Z_t is given by

$$Z_t = \frac{\Psi_1}{\Phi}\Big[Z_p + Z_c\Phi\Big], \tag{5}$$

with $\Psi_1 = (m_e/m_i)^2$ representing the correction factor that considers the cavity effect wall thickness on the total acoustic impedance, $\Phi = (N\times l^2)/(A)$ is perforation ratio, $N = 2$ is the number of perforations and A the area of the panel of the Helmholtz resonator. In Eq. (5) Z_c represents the air cavity impedance and Z_p the panel impedance, which is written as

$$Z_p = j\omega t\rho_{ef} + 2\alpha_0 R_s + j\omega\rho_0\delta, \tag{6}$$

where ρ_{ef} is the complex effective density within a perforation, which incorporates the loss of viscous energy. The perforation thickness is related to the total thickness of the resonator, i.e., $t = H - h + e$. The first term in Eq. (6) represents the effective loss of viscosity within a perforation, and the second term represents the resistive end correction by the surface, $R_s = \sqrt{2\eta\rho_0\omega}/2$. Here, $\alpha_0 = 2 + 0.96(1 - 1.14\Phi)l/t$ is the modified resistance correction coefficient, which depends on the type of perforation. The third term of Eq. (6) expresses the end correction factor, showing the effects of added mass in the neck of the perforations. For the square cross sections, $\delta = 0.85l[1 - 1.33\Phi^{1/2} - 0.07\Phi + 0.40\Phi^{3/2}]$ (Cox and D'Antonio, 2016).

Considering a panel with square perforations or arbitrary cross-section shape, the effective density is obtained as (Allard and Atalla, 2009); (Okuzono *et al.*, 2019)

$$\rho_{ef} = \rho_0\left[1 + \frac{\sigma\phi}{j\omega\rho_0}\left(\frac{-s\sqrt{(-j)}J_1\Big(s\sqrt{(-j)}\Big)}{4J_0\Big(s\sqrt{(-j)}\Big)}\Bigg/\left(1 - \frac{2J_1\Big(s\sqrt{(-j)}\Big)}{\Big(s\sqrt{(-j)}\Big)J_0\Big(s\sqrt{(-j)}\Big)}\right)\right)\right], \tag{7}$$

where $\sigma = 7\eta/(\phi\bar{r}^2)$ is the flow resistivity for the square hole, $\phi = Nl^2$, $\bar{r} = 2S/P$ is the hydraulic radius, $P = 4l$ represents the perforation perimeter and S is the cross-sectional area of the perforation. In Eq. (7) the parameter s is given as

$$s = c\sqrt{\frac{8\omega\rho_0}{\sigma\phi}}, \tag{8}$$

where $c = \sqrt{8\eta/(\sigma\phi)}/\bar{r}$ represents the shape-dependent factor.

According to the impedance transfer method, the acoustic impedance of the air cavity in Eq. (5) be written as

$$Z_c = -jZ_0\cot\Big(k_0\Psi_2 L_t\Big), \tag{9}$$

where $Z_0 = \rho_0 c_0$ is the characteristic acoustic impedance of air and $c_0 = 343$ m·s^{-1} and $k_0 = \omega/c_0$ are the sound speed and wavenumber of air, respectively; $H = h + t - e$ is the internal thickness of air cavity; $\Psi_2 = (V_c - V_n)/V_c$ represents the cavity thickness correction factor (this correction is introduced here to exclude the cavity volume occupied by the embedded necks), where $V_n = N[l^2(t-e)]$ and $V_c = WHm_i$ are the volumes of the perforations and the air cavity, respectively.

From the Eqs. (2), (5), (6) and (9), the total acoustic impedance of HAM is obtained. Considering a normal wave incidence, α can be obtained from the Eq. (1) as being

$$\alpha = 1 - \left|\frac{1 - Z_0/Z_h}{1 + Z_0/Z_h}\right|^2. \tag{10}$$

3. NUMERICAL METHOD

In this section, an numerical model using the finite element method (FEM) in the commercial software COMSOL Multiphysics version 6.1 is presented. A stationary harmonic behavior was assumed, that is, the behavior of the particles velocity and acoustic pressure field in the frequency domain was acquired. The numerical model was built by the coupling the acoustic-thermoacoustic physics. The Fig. 2 shows the mesh of the numerical model, sound hard boundary condition is assumed, where the isothermal non-slip conditions are applied in the model, such as v = 0, T = 0, where v and T are the velocity and temperature in the region absorber air. A plane wave radiation condition to simulate incident waves with pressure amplitude of 1 Pa is established.

We can been see, there are four domains in the model: (1) the perfectly matched layer (PML), that simulates an infinite air domain, which makes the boundary of the sound field free from spurious reflections; (2) the acoustic domain for the air volume facing the absorber's surface, where the Helmholtz equation is solved; (3) the Helmholtz resonator with thermoacoustics domain, where the Navier-Stokes, continuity, and energy equations are solved (do N. Almeida *et al.*, 2023) (do N. Almeida *et al.*, 2021b), (Vergara *et al.*, 2022); and (4) the poroacoustic domain of the porous layer, where the Helmholtz equation is solved and the porous material is described by the JCAL model. Finally, the surface impedance at the interface of the HAM (solid orange line) is calculated by

$$Z_{\text{fem}} = \frac{\langle P_{\text{fem}} \rangle}{\langle U_{\text{fem}} \rangle} \tag{11}$$

with $\langle P_{\text{fem}} \rangle$ and $\langle U_{\text{fem}} \rangle$ representing the average sound pressure and the average normal velocity particles at the surface interface, respectively. Therefore, the α can be determined by replacing Z_h for Z_{fem} in Eq. (10).

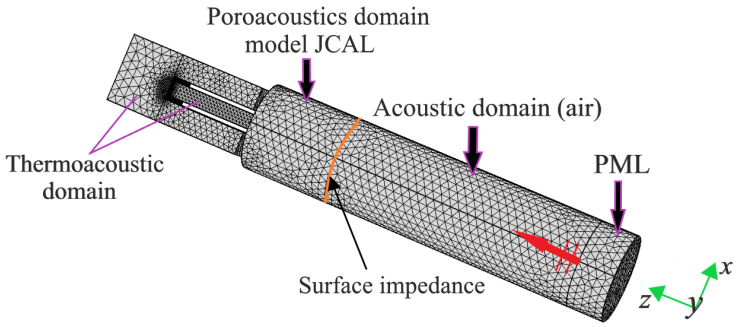

Figure 2. Finite element model of HAM.

4. EXPERIMENTAL TESTS

The experimental performance of the HAM was carried out in a cylindrical impedance tube with a diameter of $d = 26$ mm, corresponding to a cut-off frequency of $f_c = 1.84c_0/(\pi d) = 7726$ Hz. Nevertheless, an frequency range of $100 - 3000$ Hz it will be considered in the analyzes presented here. The sample of Helmholtz resonator (HR) were manufactured by 3D fusion deposition printing technology, with a resolution of ± 0.1 mm. The HMA (foam+HR) was installed at the sample holder allowing an fit snugly into the internal diameter of the impedance tube and evaluated using the standardized transfer function method with two microphones (ISO10534-2, 1998). Two 1/2 inch condenser microphones (Bruel & Kjaer type 4189-A) recorded the sound pressure, and a data acquisition system (Bruel & Kjaer LAN-XI Type 3160-B-042) was employed to obtain and process the signals. The distance between thr microphones is 24 mm, with the farthest microphone remaining 66 mm from the sample surface. In the moment of execution of the experiments, the air temperature was 20°C.

5. RESULTS AND DISCUSSION

In this sectiom, we present the results of the HAM behavior. Initially, the theoretical and numerical results are presented with a discussion about the sound energy control in a wide frequency domain as well as the mechanism underling its performance. Finally, an experimental validation and bandwidth factor are presented.

5.1 Theoretical and numerical results

The behavior of the hybrid acoustic material with melamine (HAM-M) and PET wool layers (HAM-W) was carried out. The acoustic and geometric parameters used in the analyzes are shown in Tables 1 and 2, respectively. First, figure3

presents sound absorption coefficient of the parts of HAM-M, that is, of the Helmholts resonator (HR) with embedded necks and of the PET wool layer individually. I can be seen the HR present a sound absorption peak at 460 Hz with 87% of magnitude. The thickness of the HR is $H = h+t = 40$mm, the correspond to $\approx \lambda/19$, this evidences that the resonator have the subwavelength scale. On the other hand, the PET wool present an sound energy control $\geq 50\%$ in the frequency range between $1.500 - 3.600$ Hz.

Table 1. Acoustic parameters of the PET (polyethylene terephthalate) wool and melamine with thickness $L_f = 25$ mm obtained from Kulakauskas *et al.* (2016) and Barbosa *et al.* (2017).

ϕ [%]	α_∞ [-]	σ_r [Ns·m^{-4}]	Λ [μm]	$\hat{\Lambda}$ [μm]
0.9	1.0	9227	362.1	362.2
0.9	1.0	12627	91.0	148.0

Table 2. Geometric parameters (in mm) used in the manufactured of the HAM, where a and b are fixed at 1.0 mm.

Parameters	L	m_e	h	t	l	a
HAM-W and HAM-M	20.0	16.0	15.0	25.0	3.0	4.5

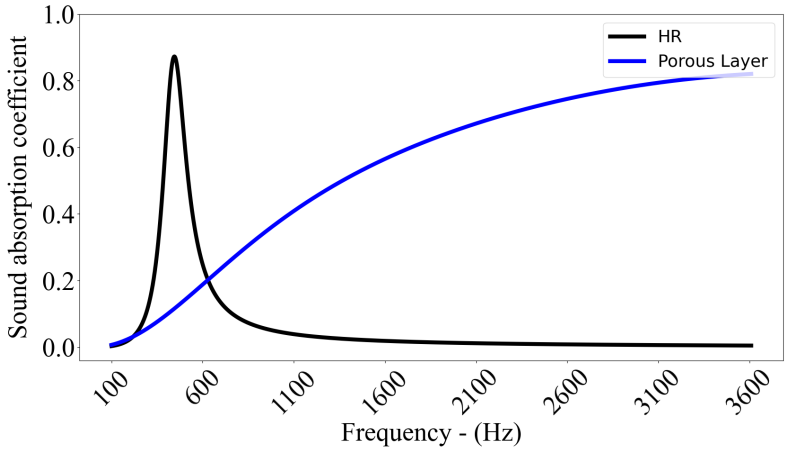

Figure 3. Theoretical behavior of sound absorption coefficient of the Helmholtz resonator and the PET wool.

Figure 4 present the numerical and theoretical behavior of the sound absorption coefficient of the combined system proposed, i. e., of the HAM-W and HAM-M. See that the behavior of absorber represent the sobreposition of the curves of the differents material combined. Furthermore, an good agreement between the methods is observed in both configurations. Regardless of the type of porous material used, the low frequency absorption peak does not change considerably.

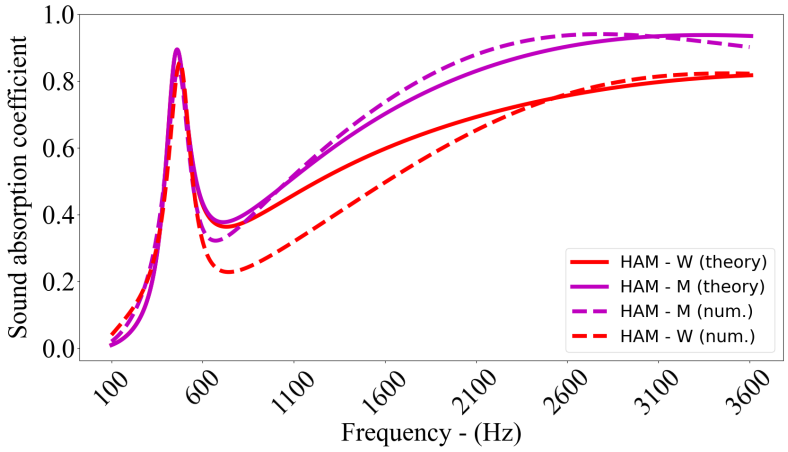

Figure 4. Theoretical and numerical behavior of sound absorption coefficient of the HAM-M and HAM-W.

However, although the porous layers used have the same thickness $L_f = 25$mm, in the mid-high frequences region the melamine presents better sound absorption control that the PET wool, this behavior is due mainly the influence of the flow resistivity. The impedance (Z_h) of the HAM can be used to better understanding the behavior of the absorber. The real and imaginary parts of the total normalized acoustic impedance of the HAM-M and HAM-W are shown in Figure 5. It can be seen that above 1.600 HZ, the real part oh the HAM-M converge firstly to unity in coparison to HAM-W. The peaks evidenced at 650 Hz in the real part represents the valley in the curves of sound absorption coefficient. With relation to the last frequency peak (460 Hz), in both configurations the real part os 0.52 while imaginary part is 0.1 and this results corroborates the behavior presents of the Figure 4. The imaginary part of the HAM-W and HAM-M is closer to zero in most of the mid-high-frequency region; this is due that $Z_t >> Z_f$, which means that the foam mainly contributes to sound absorption and the HR simply works as a rigid support. On the other hand, in the low-frequency peak (460 Hz) the imaginary part is closer to zero this is due to the coupling effect of the HR with the porous layer.

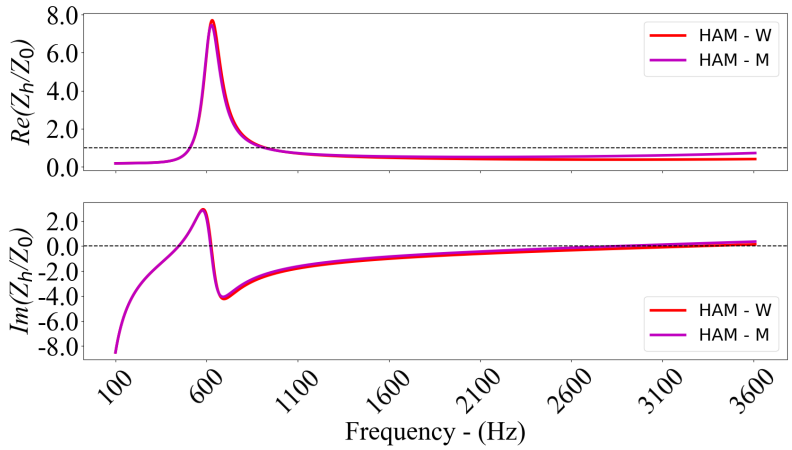

Figure 5. Behavior of the total normalized acoustic impedance of HAM.

Based on numerical simulation model, the underlying physical mechanism to the broadband sound absorption performance of the HAM-W and HAM-M was also explored by the acoustic pressure field distribution (color map) and of spatial distribution of the instantaneous particle velocity at three frequency (460 Hz, 800 Hz and 3.500 Hz), as illustrated in Figure 6. At 460 Hz, the sound absorption is dominated by the HR, the acoustic pressure at the input surface (PET wool), and at the end air cavity of the HAM-W and HAM-M is aproximately five and four times higher than the field incident (1 Pa). When the sound waves is initially incident and propagates along the PET wool, a plane wavefront (black arrows) is observed, as is the case when the porous layer is supported by a rigid wall. Nevertheless, at the end of the porous layer and consequently at the entrance of the HR, the wavefront is strongly distorted to propagate in the perforations of the HR, this behavior is due to different conditions of matching of reactances between the porous layer and the surface of the HR (Vergara *et al.*, 2022). The air movement in the perforations characterizes a strongly induced wave propagation causing much of the energy dissipation at the the operating frequency.

At 800 Hz, the sound energy is almost completely absorbed by the PET wool (see Figure 5) and the distribution of the acoustic pressure decreases from the porous layer to the perforations of the HR. This behavior means that the porous layer reduces the reactance of the system and dominates the sound absorption. Furthermore, in this frequency the propagation of sound waves (black arrows) in the absorber occurs with the phase reversed when compared to the frequency 460 Hz. Finally, at 3500 Hz, the waves propagate with inverted phases between the different materials that composed of the HAM, that is, a plane wavefront is observed along the PET wool, and in the opposite direction, the wavefront is strongly distorted from the air cavity for the HR perforations. It can be seen tthat the sound energy is fully absorbed by the porous layer, and the sound pressure distribution decreases from the ened of the porous layer to the end of the air cavity of the HR. At this frequency the layer of the porous material adjusts the reactance of the system and dominates the sound absorption.

5.2 Experimental results

For experimental validation, one sample of the HAM absorber were fabricated by 3D printing technology using the fusion deposition technique, a sketch of the HR manufactured and a photograph of the HR and PET wool that composes of the HAM-W-2 is shown in Figure 7. All adopted acoustic and geometric parameter are shown in Tables 3 and 4, respectively. See that the HAM-W-2 presents two different HR coupled in the same structure, thus, the total acoustic impedance of the system is obtained by the associated parallel impedance, i. e.,

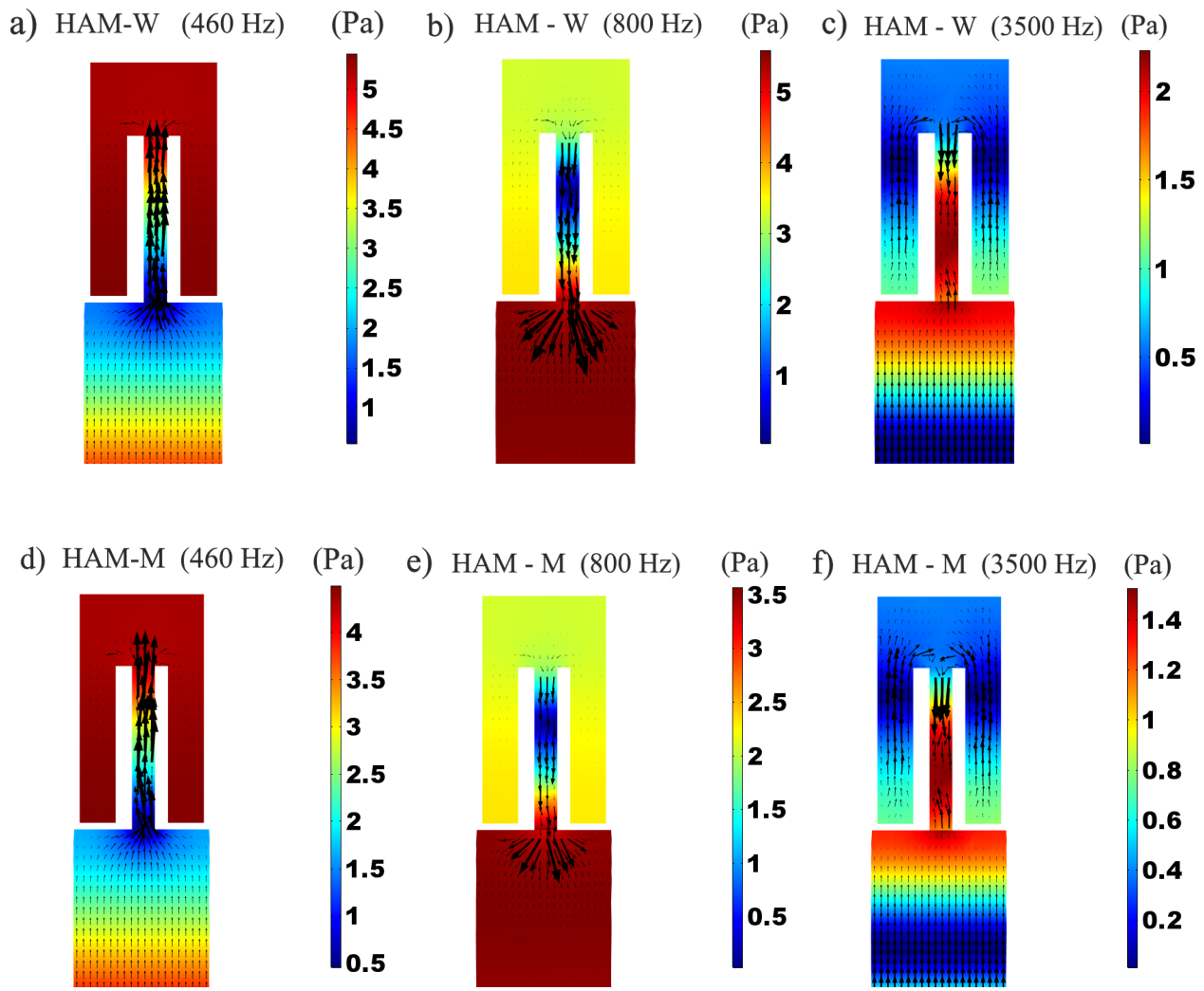

Figure 6. The pressure field (color map) and distribution of the instantaneous particle velocity (black arrows): a) - c) HAM-W and d) - f) HAM-M.

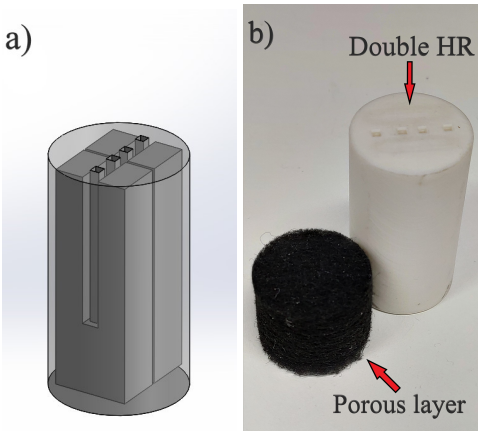

Figure 7. a) Internal 2D view of the modified Helmholtz resonator and b) parts of the HAM-W-2 proposed for the experiment.

$$Z_T = \left[\frac{1}{S}\left(\frac{S_1}{Z_{t_1}} + \frac{S_2}{Z_{t_2}}\right)\right]^{-1}, \tag{12}$$

where $S_1 = S_2$ is the area of each HR and S is the total area of the system.

Figure 8 presents sound absorption comparison between the theoretical and experimental results of absorber. Theo-

Table 3. Acoustic parameters of the PET (polyethylene terephthalate) wool with thickness $L_f = 25.0$ mm.

ϕ [%]	α_∞ [-]	σ_r [Ns·m^{-4}]	Λ [μm]	$\hat{\Lambda}$ [μm]
0.9	1.0	4683	362.1	362.2

Table 4. Geometric parameters (in mm) used in the manufactured of the HAM, where a and b are fixed at 1.0 mm.

Parameters	L	m_e	h	t	l	a
HAM-W-2	10.0	16.0	26.0	19.0	2.0	5.0
	10.0	16.0	16.0	29.0	1.9	5.0

retical result of the PET wool with the same thickness ($L_f = 61.5$ mm) of HAM-W-2 and of the double HR are also plotted. A good agreement can be observed between theoretical and experimental results of the HAM-W-2, with respective low-frequency absorption peaks at 0.95 (300 Hz), 0.98 (365 Hz) for theory and 0.80 (330 Hz) and 0.82 (388 Hz) for the measurement. We can be seen small discrepancies between the experimental and theoretical results exist, this behavior is due to the imprecision of the manufactured sample, mainly caused by the internal non-uniformity of the square perforation of the modified Helmholtz resonator (Vergara *et al.*, 2022; do N. Almeida *et al.*, 2021a). At mid-high-frequency region the theoretical and experimental results converge.The advantage of HAM-W-2 for the PET wool with the same thickness (61.5 mm) is the prominence of the low-frequency peak absorption since the proposed absorber can be tuned to the lowest target frequency that is aimed to attenuate without modifying the absorption from other frequencies. Note that the peak low-frequency absorption of HAM-W-2 can be tuned at without changing the performance at high frequencies maintaining the porous layer thickness fixed. Thus, the proposed absorber presents low-frequency sound absorption and broadband absorption, the low-frequency peak being adjustable by the thickness of the HR. The total thickness of the HAM-W-2 is $\approx 1/17$ of the sound wavelength of smaller frequency (330 Hz).

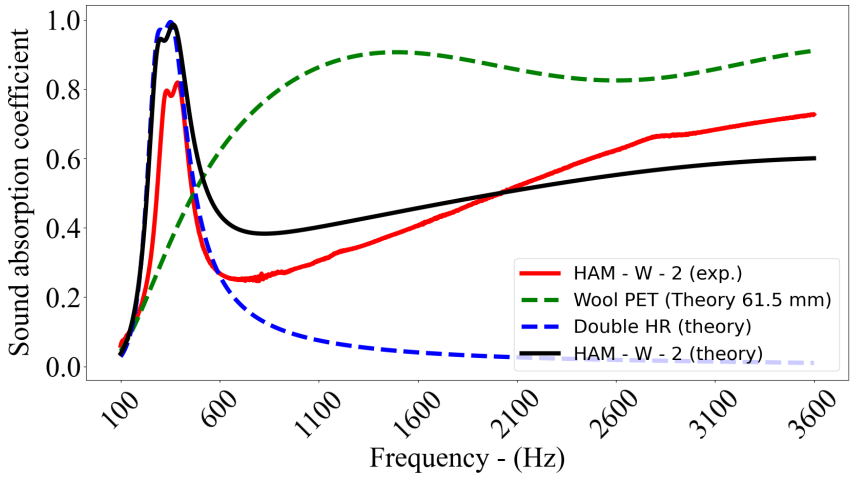

Figure 8. Sound absorption coefficient of the HAM-W-2 with 25 mm thickness of the PET wool layer and behavior of the PET wool with 61.5 mm.

The broadband absorption property for the HAM proposed is evaluated by the broadband factor (Q_α) (Climente *et al.*, 2012), which define the average value of the absorption coefficient within a specific bandwidth, that is,

$$Q_\alpha = \frac{1}{\Delta f}\int_{f_i}^{f_f} \alpha(f)df \tag{13}$$

with $\Delta f = f_f - f_i$ being the bandwidth and f_f and f_i are the upper and lower frequencies of analysis, respectively. Table 5 shows all the result obtained between 100 and 3600 Hz, and for purposes of comparison, the absorption properties of HR and of the PET wool were determined. The factor Q_α of HAM-W-2 theoretical and experimental presentes values nearly, that corroborates the good agreement between results of the broadband absorption. An Q_α experimental of the HAM-W-2 76.47% greater than the Q_α of HR is observed, onthe other hand, the Q_α theoretical of the HAM-W-2 is 77.39% greater tha Q_α of HR. The Q_α of PET woll with 61.5 mm is 36.8% greater than the Q_α experimental of the HAM-W-2. We can seen that comparatively, HAM-W-2 performs better in the low-frequency region than foam with 61.5 mm. Therefore, the HAM-W-2 sample has better lowfrequency and broadband sound absorption performance than porou layer and HR. In addition, the modular characteristics of the HAM show the possibility of adjusting the sound

Table 5. Experimental and theoretical Q_α absorption parameters of different materials analyzed between 100 and 3600 Hz.

Absorbent material	Q_α
HAM-W-2 (theoretical)	0.513
HAM-W-2 (experimental)	0.493
PET wool with $L_f = 61.5$ mm (theoretical)	0.780
HR (theoretical)	0.116

absorption in the mid-high frequency regions by the thickness of the foam and in the low-frequency by adjusting mainly the dimensions (l) or the thickness (t) of square perforations of the HR panel, maintaining the total absorber structure with the same thickness.

6. CONCLUDING REMARKS

In this work, a hybrid acoustic material for sound energy control in a wide frequency domain was proposed. Broadband sound absorption was obtained combined a modified Helmholtz resonator and a porous layer. The type of the porous material and it is thickness produce a strong influence on the sound energy control. The experimental work allowed us to successfully validate the theoretical model based on the equivalent fluid concept. Using numerical sinulations the behavior of the broadband absorption was detailed and explained by the reactance matching conditions, of the pressure field and particle velocity between the two materials that composed of the hybrid acoustic material. The parameter Q_α was used and revealed that the absorber proposed presents more design possibilities to adjust the broadband absorption spectrum. Finally, the proposed hybrid absorber allows applications to sound energy control bandwidth at low-frequency.

7. ACKNOWLEDGEMENTS

This research has been supported by the Graduate Program in Mechanical Engineering (POSMEC) and the Laboratory of Vibrations and Acoustics of the Federal University of Santa Catarina, Brazil. The Gildean do N. Almeida author is grateful for funding from the Coordination of Superior Level Staff Improvement (CAPES), Brazil. The authors Lucas R. Zanatta and Kleyton K. Zimmermann are grateful for funding from Institutional Scientific Initiation Scholarship Program (PIBIC) and Institutional Program of Initiation Scholarships in Technological Development and Innovation (PIBITI), respectively.

8. REFERENCES

Allard, J. and Atalla, N., 2009. *Propagation of sound in porous media: modelling sound absorbing materials 2e*. John Wiley & Sons.

Barbosa, L.R. *et al.*, 2017. "Uso de materiais acústicos metálicos em filtros de descarga de sistemas de refrigeração".

Cao, L., Fu, Q., Si, Y., Ding, B. and Yu, J., 2018. "Porous materials for sound absorption". Vol. 10, pp. 25–35. doi:10.1016/j.coco.2018.05.001.

Champoux, Y. and Allard, J.F., 1991. "Dynamic tortuosity and bulk modulus in air-saturated porous media". Vol. 70, No. 4, pp. 1975–1979. doi:10.1063/1.349482.

Climente, A., Torrent, D. and Sánchez-Dehesa, J., 2012. "Omnidirectional broadband acoustic absorber based on metamaterials". *Applied Physics Letters*, Vol. 100, No. 14, p. 144103.

Cobo, P. and Simón, F., 2019. "Multiple-layer microperforated panels as sound absorbers in buildings: A review". Vol. 9, No. 2, p. 53. doi:10.3390/buildings9020053.

Cox, T. and D'Antonio, P., 2016. *Acoustic Absorbers and Diffusers*. CRC Press. doi:10.1201/9781315369211.

de Moraes, E.G., Sangiacomo, L., Stochero, N., Arcaro, S., Barbosa, L., Lenzi, A., Siligardi, C. and de Oliveira, A.N., 2019. "Innovative thermal and acoustic insulation foam by using recycled ceramic shell and expandable styrofoam (eps) wastes". *Waste Management*, Vol. 89, pp. 336–344. doi:10.1016/j.wasman.2019.04.019.

do N. Almeida, G., Vergara, E.F., Barbosa, L.R. and Brum, R., 2021a. "Low-frequency sound absorption of a metamaterial with symmetrical-coiled-up spaces". Vol. 172, p. 107593. doi:10.1016/j.apacoust.2020.107593.

do N. Almeida, G., Vergara, E.F., Barbosa, L.R., Lenzi, A. and Birch, R.S., 2021b. "Sound absorption metasurface with symmetrical coiled spaces and micro slit of variable depth". Vol. 183, p. 108312. doi:10.1016/j.apacoust.2021.108312.

do N. Almeida, G., Vergara, E.F., Lenzi, A., Alves, Á.S. and de Jesus, J.C.O., 2023. "Low-frequency broadband sound absorption based on cantor fractal porosity". Vol. 133, No. 23. doi:10.1063/5.0150998.

Doutres, O., Salissou, Y., Atalla, N. and Panneton, R., 2010. "Evaluation of the acoustic and non-acoustic properties of sound absorbing materials using a three-microphone impedance tube". Vol. 71, No. 6, pp. 506–509. doi:

10.1016/j.apacoust.2010.01.007.

Duan, M., Yu, C., Xu, Z., Xin, F. and Lu, T.J., 2020. "Acoustic impedance regulation of helmholtz resonators for perfect sound absorption via roughened embedded necks". Vol. 117, No. 15, p. 151904. doi:10.1063/5.0024804.

Dupont, T., Leclaire, P., Sicot, O., Gong, X.L. and Panneton, R., 2011. "Acoustic properties of air-saturated porous materials containing dead-end porosity". Vol. 110, No. 9, p. 094903. doi:10.1063/1.3646556.

Guo, Y., Allam, S. and Åbom, M., 2008. "Micro-perforated plates for vehicle applications". In *37th International Congress and Exhibition on Noise Control Engineering, Shanghai, China October, 2008*.

Huang, S., Fang, X., Wang, X., Assouar, B., Cheng, Q. and Li, Y., 2019. "Acoustic perfect absorbers via helmholtz resonators with embedded apertures". Vol. 145, No. 1, pp. 254–262. doi:10.1121/1.5087128.

ISO10534-2, 1998. "Acoustics—determination of sound absorption coefficient and impedance in impedance tubes—part 2: Transfer-function method".

Ji, G., Fang, Y. and Zhou, J., 2020. "Porous acoustic metamaterials in an inverted wedge shape". Vol. 36, p. 100648. doi:10.1016/j.eml.2020.100648.

Johnson, D.L., Koplik, J. and Dashen, R., 1987. "Theory of dynamic permeability and tortuosity in fluid-saturated porous media". Vol. 176, No. -1, p. 379. doi:10.1017/s0022112087000727.

Kim, B.S. and Park, J., 2018. "Double resonant porous structure backed by air cavity for low frequency sound absorption improvement". Vol. 183, pp. 545–549. doi:10.1016/j.compstruct.2017.06.027.

Kulakauskas, F.L.V.Q. *et al.*, 2016. "Avaliação do uso de materiais porosos na perda de transmissão de painéis duplos".

Lafarge, D., Lemarinier, P., Allard, J.F. and Tarnow, V., 1997. "Dynamic compressibility of air in porous structures at audible frequencies". Vol. 102, No. 4, pp. 1995–2006. doi:10.1121/1.419690.

Li, D., Chang, D. and Liu, B., 2017. "Enhanced low- to mid-frequency sound absorption using parallel-arranged perforated plates with extended tubes and porous material". Vol. 127, pp. 316–323. doi:10.1016/j.apacoust.2017.06.019.

Li, H., Wu, J., Yan, S. and Mao, Q., 2023. "Design and study of broadband sound absorbers with partition based on micro-perforated panel and helmholtz resonator". Vol. 205, p. 109262. doi:10.1016/j.apacoust.2023.109262.

Li, J., Wang, W., Xie, Y., Popa, B.I. and Cummer, S.A., 2016. "A sound absorbing metasurface with coupled resonators". Vol. 109, No. 9, p. 091908. doi:10.1063/1.4961671.

Li, X., Liu, B. and Chang, D., 2021. "An acoustic impedance structure consisting of perforated panel resonator and porous material for low-to-mid frequency sound absorption". Vol. 180, p. 108069. doi:10.1016/j.apacoust.2021.108069.

Li, Y., Yan, J. and Peng, Y., 2022. "Multiscale porous with coiled-up channel for low-frequency broadband sound absorption". Vol. 232, p. 107622. doi:10.1016/j.ijmecsci.2022.107622.

Liu, X., Yu, C. and Xin, F., 2021. "Gradually perforated porous materials backed with helmholtz resonant cavity for broadband low-frequency sound absorption". Vol. 263, p. 113647. doi:10.1016/j.compstruct.2021.113647.

Maa, D.Y., 1987. "Microperforated-panel wideband absorbers". Vol. 29, No. 3, p. 77. doi:10.3397/1.2827694.

Mahesh, K., Ranjith, S.K. and Mini, R.S., 2021. "Inverse design of a helmholtz resonator based low-frequency acoustic absorber using deep neural network". Vol. 129, No. 17, p. 174901. doi:10.1063/5.0046582.

Mei, J., Ma, G., Yang, M., Yang, Z., Wen, W. and Sheng, P., 2012. "Dark acoustic metamaterials as super absorbers for low-frequency sound". Vol. 3, No. 1. doi:10.1038/ncomms1758.

Okuzono, T., Nitta, T. and Sakagami, K., 2019. "Note on microperforated panel model using equivalent-fluid-based absorption elements". Vol. 40, No. 3, pp. 221–224. doi:10.1250/ast.40.221.

Vergara, E.F., Almeida, G.N., Barbosa, L.R., Lenzi, A. and de Sousa, A.C., 2022. "Broadband and low-frequency sound absorption of modified helmholtz resonator combined with porous layer addition". Vol. 132, No. 13, p. 135114. doi:10.1063/5.0108807.

Xu, Q., Qiao, J., Ren, Z., Sun, J., Zhang, G. and Li, L., 2022. "Multi synergistic coupling design for broadband sound absorption based on compact porous composite embedded with massless membrane resonator". Vol. 286, p. 115312. doi:10.1016/j.compstruct.2022.115312.

Zhang, W. and Xin, F., 2023. "Coiled-up structure with porous material lining for enhanced sound absorption". p. 108480. doi:10.1016/j.ijmecsci.2023.108480.

Zhao, H., Wang, Y., Wen, J., Lam, Y.W. and Umnova, O., 2018. "A slim subwavelength absorber based on coupled microslits". Vol. 142, pp. 11–17. doi:10.1016/j.apacoust.2018.08.004.

Zhao, H., Wang, Y., Yu, D., Yang, H., Zhong, J., Wu, F. and Wen, J., 2020. "A double porosity material for low frequency sound absorption". Vol. 239, p. 111978. doi:10.1016/j.compstruct.2020.111978.

9. RESPONSIBILITY NOTICE

The authors Gildean d N. Almeida, Erasmo F. Vergara, Leandro R. Barbosa, Lucas R. Zanatta, Kleyton K. Zimmermann, Robson Z. Mikulski and Victor H. P. Bahú are solely responsible for the printed material included in this paper.